Int. J. Heat Mass Transfer. Vol. 21, pp. 1565–1579
Pergamon Press Ltd 1978. Printed in Great Britain

TRANSIENT FLOW AND HEAT TRANSFER OF LIQUID SODIUM COOLANT IN THE OUTLET PLENUM OF A FAST NUCLEAR REACTOR

NICHOLAS C. G. MARKATOS
CHAM Limited, 40 High Street, Wimbledon, London SW19 5AU, England

(*Received* 28 *November* 1977 *and in revised form* 15 *March* 1978)

Abstract—A calculation procedure for axisymmetric elliptic flows is applied to predict the transient velocity and temperature fields of a heavy fluid jet issuing vertically into a volume of relatively light fluid. This situation arises in the outlet plenum of a Liquid-Metal-Cooled Fast Breeder Reactor (LMFBR) during reactor transients. The time averaged conservation equations for momenta and heat transfer were solved on a CDC 6600 digital computer for various plenum inlet transients, along with a two-equation model of turbulence and proper modelling of the buoyancy terms. Predictions are presented of flow and heat transfer in the form of velocity vector plots and temperature contours. Predictions are in qualitative agreement with expectations, invariably establishing that the flow by-passes the outlet plenum.

NOMENCLATURE

C_1, C_2, C_μ, constants in the turbulence model;
C_p, specific heat at constant pressure [J/kg °K];
g, gravitational acceleration [m/s^2];
G, generation term for turbulent kinetic energy;
$J_{\phi,j}$, diffusional flux of ϕ;
h, stagnation enthalpy [J/kg];
k, turbulence kinetic energy [m^2/s^2];
l, length scale of turbulence [m];
p, static pressure [N/m^2];
r, local radius of curvature [m];
S_ϕ, source (or sink) term for the ϕ-variable;
t, time coordinate [s];
T, temperature [K];
u_i, the velocity component in the i-direction; $u_1 \equiv u$ x-direction velocity, $u_2 \equiv v$ r-direction velocity [m^2/s];
x_i, set of two mutually-orthogonal space coordinates [m].

Greek symbols

β, coefficient of volumetric expansion [K^{-1}];
Γ_ϕ, the coefficient of diffusion for ϕ;
δ_{ji}, Kronecker delta;
ε, dissipation rate of turbulence energy [m^2/s^3];
κ, Prandtl's constant;
μ, molecular viscosity [kg/ms];
ν, kinematic viscosity [m^2/s];
ρ, density [kg/m^3].

Subscripts and symbols

D/Dt, substantial derivative;
eff, effective; it stands for enhanced turbulent properties;
l, laminar;
t, turbulent;
x', turbulent fluctuating component of the quantity x;
$\langle\ \rangle$, averaging symbol.

1. INTRODUCTION

1.1. *The problem considered*

A heavy fluid jet issuing vertically into a volume of relatively light fluid will not rise indefinitely but will reach some maximum height and subsequently flow downward.

This type of flow apart from its general theoretical interest, is also of great importance to the reactor design engineer, since it arises in the outlet plenum of a Liquid-Metal-Cooled Fast Breeder Reactor (LMFBR) during reactor transients.

In the primary coolant loop of the reactor, sodium coolant enters the pressure vessel through three inlet nozzles and flows upward from an inlet plenum, through the reactor core and other components and instrument trees requiring heat removal, into an outlet plenum. Under steady state isothermal operation, sodium enters the plenum through an inlet structure, and after mixing within the plenum exits through three outlet nozzles. During a reactor transient, the plenum experiences an abrupt decrease in the entering temperature and consequently an increase in the entering fluid density. This temperature decrease is accompanied in a normal reactor transient by an exponential flow coastdown to about 10% of the initial flow-rate. The design of the outlet plenum and components in a LMFBR reactor, is largely governed by their response to thermal transients. The large fluid volume in the outlet plenum provides a region in which thermal transients at the inlet can be significantly mitigated, due to flow mixing in the plenum.

If, however, the cooler, denser sodium has insufficient inertia upon entering the plenum to overcome the negative buoyancy forces, the incoming fluid will immediately be forced downward and outward toward the exit nozzles, thus short-circuiting the plenum and creating a stratified flow pattern. Poten-

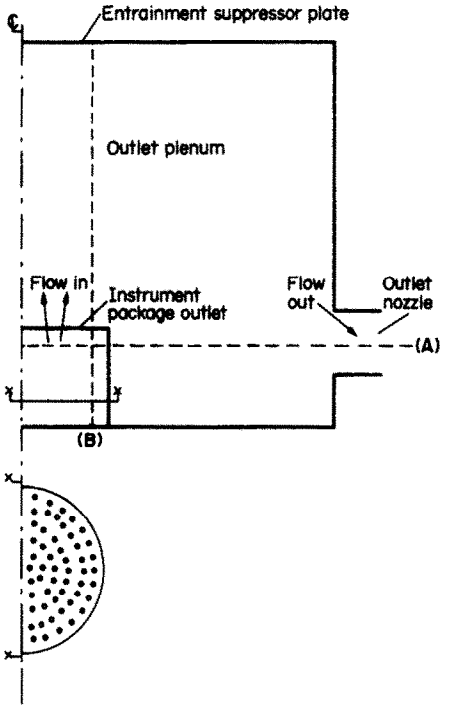

FIG. 1. The flow domain (schematic).

tial areas of stagnation could result in temperature differentials in the outlet region, which could, in turn, cause structural or functional damage to reactor components.

1.2. *Present work*

In the present study, the elliptic differential equations governing transient two-dimensional turbulent flow are solved by a procedure first proposed by Patankar and Spalding [1] for parabolic flows.

Figure 1 presents a simplified sketch of the desired outlet plenum, in the idealised form adopted for the present computations. The path of the coolant flow (liquid sodium) is vertically upward in the core zone. The flow then deflects horizontally at, or near the pool cover–gas interface, passes outward at the top and then passes downward near the vessel wall, toward the outlet nozzles.

The present model includes simulated core outlet (the actual open area being less than the total cross-sectional area illustrated in the above figure), simulated plenum outlet and simulated pool cover interface.

1.3. *Outline of the paper*

The mathematical formulation and the calculation procedure, which is of the finite-difference type, are described in Section 2. The results of the computations and discussion of these results are presented in Section 3. Section 4 discusses possible further developments.

2. MATHEMATICAL STATEMENT OF THE PROBLEM

2.1. *The geometry and governing differential equations*

The physical situation illustrated in Fig. 1, may be conveniently described in cylindrical coordinates (r, x) as a two-dimensional axisymmetric field. Accordingly, the three outlet nozzles will be modelled as a continuous annular slot of the same area as the three outlet nozzles, and with its centre at the proper elevation. The upper surface of the vessel is assumed to be a solid surface in contact with the plenum fluid and located at the same elevation as the entrainment suppressor plate.

This flow depends on two space variables; but, there is no dominant direction of flow. Such a flow can be described mathematically by partial differential equations of the elliptic type.

Under most circumstances the flow field within the plenum will be turbulent. To account for turbulence the two-equation model of Harlow and Nakayama [2] as developed by Launder and Spalding [3–5], is included. This model uses as dependent variables the kinetic energy of turbulence (k) and its dissipation rate (ε). Although this model had been devised initially for thin shear flows, it has been used successfully for other types of flow as well (see for example, Spalding and Tatchell [6], Gosman *et al.* [7], and Khalil *et al.* [8]).

Within the above framework, the independent variables are the axial (x) and radial (r) components of a cylindrical-polar coordinate system and the time (t); the dependent variables (time-averaged values) are the two velocity components (u, v), the static pressure (p), the stagnation enthalpy* (h) and the two turbulence quantities (k, ε).

The differential equations for the above dependent variables follow:

(a) *Continuity.*

$$\frac{\partial \rho}{\partial t} + \frac{1}{r}\left[\frac{\partial}{\partial x}(\rho r u) + \frac{\partial}{\partial r}(\rho r v)\right] = 0. \tag{1}$$

(b) *Momentum.* In a Cartesian system Newton's second law is expressed in tensor notation by:

$$\frac{\partial(\rho u_i)}{\partial t} + \frac{\partial(\rho u_j u_i)}{\partial x_j} = Su_i + \frac{\partial \tau_{ji}}{\partial x_j} \tag{2}$$

where: u_i is the velocity in the i-direction; x_j form the set of two mutually-orthogonal space coordinates; τ_{ji} is the complete stress tensor; and Su_i is the source (and/or sink) of u_i.

In a turbulent flow the stress tensor may be expressed as:

$$\tau_{ji} = -p\delta_{ji} + \mu\left(\frac{\partial u_i}{\partial x_j} + \frac{\partial u_j}{\partial x_i}\right) - \overline{\rho u_i' u_j'} \tag{3}$$

where: μ is the laminar viscosity; $'$ denotes fluctuating quantities; $-$ denotes a time average; and δ_{ji} is the Kronecker delta.

Under the Boussinesq hypothesis we have:

$$\overline{\rho u_i' u_j'} = -\mu_t\left(\frac{\partial u_i}{\partial x_j} + \frac{\partial u_j}{\partial x_i}\right) + \tfrac{2}{3}k\delta_{ij} \tag{4}$$

where k is the turbulence kinetic energy ($\overline{\frac{1}{2}u_i' u_i'}$) and μ_t is the turbulent viscosity.

Substituting (3) and (4) into (1) and providing for axisymmetrical flows, we finish up with:

$$\frac{\partial(\rho u)}{\partial t}+\frac{1}{r}\left[\frac{\partial}{\partial x}(\rho uru)+\frac{\partial}{\partial r}(\rho vru)-\frac{\partial}{\partial x}\times\left(r\mu_{\text{eff}}\frac{\partial u}{\partial x}\right)-\frac{\partial}{\partial r}\left(r\mu_{\text{eff}}\frac{\partial u}{\partial r}\right)\right]=-\frac{\partial p}{\partial x}+S_u \quad (5)$$

and

$$\frac{\partial(\rho v)}{\partial t}+\frac{1}{r}\left[\frac{\partial}{\partial x}(\rho urv)+\frac{\partial}{\partial r}(\rho urv)-\frac{\partial}{\partial x}\times\left(r\mu_{\text{eff}}\frac{\partial v}{\partial x}\right)-\frac{\partial}{\partial r}\left(r\mu_{\text{eff}}\frac{\partial v}{\partial r}\right)\right]=-\frac{\partial p}{\partial r}+\mu_{\text{eff}}\frac{v}{r^2}+S_v \quad (6)$$

where μ_{eff} is the local effective viscosity

$$(\mu+\mu_t)$$

and S represents the source (sink) terms. For a Newtonian fluid, assumed to have zero divergence of the mass velocity vector, they may be written as:

$$S_u=\frac{1}{r}\left[\frac{\partial}{\partial x}\left(r\mu_{\text{eff}}\frac{\partial u}{\partial x}\right)+\frac{\partial}{\partial r}\left(r\mu_{\text{eff}}\frac{\partial v}{\partial x}\right)\right]+\rho\beta(T-T_m)g_x+2\mu_{\text{eff}}u\frac{\partial}{\partial x}\left(\frac{1}{r}\right) \quad (7)$$

$$S_v=\frac{1}{r}\left[\frac{\partial}{\partial x}\left(r\mu_{\text{eff}}\frac{\partial u}{\partial r}\right)+\frac{\partial}{\partial r}\left(r\mu_{\text{eff}}\frac{\partial v}{\partial r}\right)\right]+2\mu_{\text{eff}}v\frac{\partial}{\partial x}\left(\frac{1}{r}\right). \quad (8)$$

The buoyancy forces caused by changes in volume, which are associated with temperature differences, are treated as impressed body forces and appear in (7) as:

$$\rho\beta(T-T_m)g_x \quad (9)$$

where: ρ is density; β is the coefficient of volumetric expansion; g_x is the x-component of the gravitational acceleration; and T_m is an average temperature over the whole flow field.

(c) *Energy conservation.* In tensor notation,

$$\frac{\partial(\rho u_j h)}{\partial x_j}=S_h+\frac{\partial J_{h,j}}{\partial x_j} \quad (10)$$

where $J_{h,j}$ is the flux of the stagnation enthalpy (h) and S_h is the source (or sink) of h.

The flux of h is expressed as:

$$J_{h,j}=-\frac{\mu}{\sigma_{h,l}}\frac{\partial h}{\partial x_j}-\overline{\rho u_i' h'} \quad (11)$$

where $\sigma_{h,l}$ is the laminar Prandtl number. The turbulent flux of h is given by the "closure" relationship:

$$-\overline{\rho u_i' h'}=-\frac{\mu_t}{\sigma_{h,t}}\frac{\partial h}{\partial x_j} \quad (12)$$

where $\sigma_{h,t}$ is the turbulent Prandtl number.

Substituting (11) and (12) into (10), introducing the unsteady term and providing for axisymmetric geometries we get:

$$\frac{\partial(\rho h)}{\partial t}+\frac{1}{r}\left[\frac{\partial}{\partial x}(\rho ruh)+\frac{\partial}{\partial r}(\rho rvh)-\frac{\partial}{\partial x}\left(r\Gamma_{\text{eff},h}\frac{\partial h}{\partial x}\right)-\frac{\partial}{\partial r}\left(r\Gamma_{\text{eff},h}\frac{\partial h}{\partial r}\right)\right]=S_h \quad (13)$$

where $\Gamma_{\text{eff},h}$ is the general transport coefficient for the diffusion of h given by:

$$\Gamma_{\text{eff},h}=\frac{\mu}{\sigma_{h,l}}+\frac{\mu_t}{\sigma_{h,t}}. \quad (14)$$

For turbulent flows, neglecting kinetic heating we also have $S_h=0$.

(d) *Turbulence kinetic energy*

$$\frac{Dk}{Dt}+\langle u_j\rangle\frac{\partial k}{\partial x_j}=-\langle u_i'u_j'\rangle\frac{\partial\langle u_i\rangle}{\partial x_j}-\frac{\partial}{\partial x_j}(\langle k'u_j'\rangle)-\frac{1}{\rho}\left(\left\langle u_i'\frac{\partial p'}{\partial x_j}\right\rangle\right)+\nu\left(\frac{\partial^2 k}{\partial x_j^2}+\frac{\partial^2\langle u_i'u_j'\rangle}{\partial x_i\partial x_j}\right)-\varepsilon \quad (15)$$

(e) *Dissipation rate of turbulence*

$$\frac{D\varepsilon}{Dt}+2\nu\left(\frac{\partial^2\langle u_i\rangle}{\partial x_l\partial x_j}\left\langle u_j'\frac{\partial u_i'}{\partial x_l}\right\rangle\right)+\frac{\partial(\langle u_i\rangle)}{\partial x_j}\left(\left\langle\frac{\partial u_i'}{\partial x_l}\frac{\partial u_j'}{\partial x_l}\right\rangle\right)+\frac{\partial\langle u_j\rangle}{\partial x_l}\left(\left\langle\frac{\partial u_i'}{\partial x_l}\frac{\partial u_i'}{\partial x_j}\right\rangle\right)+2\nu\left(\left\langle\frac{\partial u_i'}{\partial x_l}\frac{\partial u_i'}{\partial x_j}\frac{\partial u_j'}{\partial x_l}\right\rangle\right)=-2\frac{\nu}{\rho}\frac{\partial}{\partial x_i}\left(\left\langle\frac{\partial u_i'}{\partial x_l}\frac{\partial p'}{\partial x_l}\right\rangle\right)-\frac{\partial}{\partial x_j}(\langle u_j'\varepsilon'\rangle)+\nu\frac{\partial^2\varepsilon}{\partial x_j^2}-2\nu^2\left[\left\langle\left(\frac{\partial^2 u_i'}{\partial x_i\partial x_j}\right)^2\right\rangle\right]. \quad (16)$$

The above equations (15) and (16) are modelled into a suitable form following Launder and Spalding [3].

2.2. *The general equation*

The above set of equations may be expressed into the single form

$$\frac{\partial}{\partial x}(\rho u\phi)+\frac{1}{r}\frac{\partial}{\partial r}(r\rho v\phi)=\frac{\partial}{\partial x}\left(\Gamma_{\text{eff},\phi}\frac{\partial\phi}{\partial x}\right)+\frac{1}{r}\frac{\partial}{\partial r}\left(r\Gamma_{\text{eff},\phi}\frac{\partial\phi}{\partial r}\right)+S_\phi. \quad (17)$$

This is the conservation equation for the transport of a property ϕ of the fluid in a two-dimensional axisymmetric domain, where S_ϕ is a collection of terms

which do not fit in the framework of the other terms and may be called the source (or sink) terms. They are defined for each dependent variable ϕ in Table (1).

In this table:

Table 1. The source terms of the conservation equation (17)

ϕ	S_ϕ
u	$-\frac{\partial p}{\partial x}+\frac{\partial}{\partial x}\left(\mu_{\text{eff}}\frac{\partial u}{\partial x}\right)+\frac{1}{r}\frac{\partial}{\partial r}\left(\mu_{\text{eff}}\frac{r\partial v}{\partial x}\right)-\frac{\partial}{\partial t}(\rho u)-(\rho-\rho_m)g_x$
v	$-\frac{\partial p}{\partial r}+\frac{\partial}{\partial x}\left(\mu_{\text{eff}}\frac{\partial u}{\partial r}\right)+\frac{1}{r}\frac{\partial}{\partial r}\left(\mu_{\text{eff}}\frac{r\partial v}{\partial r}\right)-2\mu_{\text{eff}}\frac{v}{r^2}-\frac{\partial}{\partial t}(\rho v)$
k	$G_k-\rho\varepsilon-\frac{\partial}{\partial t}(\rho k)$
ε	$\frac{\varepsilon}{k}(C_1G_k-C_2\rho\varepsilon)-\frac{\partial}{\partial t}(\rho\varepsilon)$
h	$-\frac{\partial}{\partial t}(\rho h)$

The source term G_k for k and ε is given by:

$$G_k=\mu_{\text{eff}}\left\{2\left[\left(\frac{\partial u}{\partial x}\right)^2+\left(\frac{\partial v}{\partial r}\right)^2+\left(\frac{v}{r}\right)^2\right]+\left(\frac{\partial u}{\partial r}+\frac{\partial v}{\partial x}\right)^2\right\}. \quad (18)$$

The source of h implicitly assumes that the Prandtl numbers for h and k are equal, and the flow is incompressible. This assumption is justified by the low speed of the flow.

ρ_m is an average density over the radial direction at each axial station.

C_1, C_2 are constants in the (k,ε) turbulence model.

The flow is at a sufficiently high Reynolds number, so that we can safely neglect the laminar diffusion terms in the k and ε equations. The pressure diffusion is also unlikely to play a major part.

Terms representing generation of k by the turbulence interacting with itself are ignored.

2.3. *Definitions and auxiliary relations*

The equation set is completed by the following algebraic relation, and auxiliary information:

The effective viscosity is calculated as $\mu_{\text{eff}}=\mu+\mu_t$ where $\mu_t=C_\mu\rho(k^2/\varepsilon)$; C_μ is a constant of the turbulence model. The length scale of turbulence is given by $l=C_\mu k^{3/2}/\varepsilon$.

The local effective exchange coefficients, $\Gamma_{\text{eff},\phi}$ for the transport of scalar property ϕ, are calculated from the relation:

$$\Gamma_{\text{eff},\phi}=\frac{\mu}{\sigma_{l,\phi}}+\frac{\mu_t}{\sigma_{t,\phi}}$$

where μ and $\sigma_{l,\phi}$ are the molecular viscosity and the laminar Prandtl numbers respectively, and μ_t and $\sigma_{t,\phi}$ diffusivities of mass (ε_M) and heat (ε_H) equal. The theoretical predictions, for liquid sodium and for Reynolds numbers up to 12×10^4 for the ratio $\varepsilon_H/\varepsilon_M$ obtained by various studies differ a lot. (Dwyer, [9], Tyldesley and Silver, [10], Borishanski and Zablotskaya, [11].)

A comprehensive comparison among various models of predicting the relationship between the turbulent transfer of momentum and a passive contaminant such as heat or dissolved matter, is given by Reynolds [12]. It is shown there, that even for liquid metals $(Pr\ll1)Pr_t\to1$ for $Re\to\infty$, and this is the value used herein.

The value of the Prandtl number for k is taken as 0.9 and for ε is derived from the relation $\kappa^2/(C_\mu)^{1/2}(C_2-C_1)$ where κ is the Von Karman constant ($=0.42$).

In the problem under consideration, temperature differences bring about differences in density. It is then necessary, to include buoyancy forces in the equation of motion caused by changes in volume which are associated with the temperature differences. These forces are treated as impressed body forces, and appear in the source term of the u-momentum equation as: $(\rho-\rho_m)g_x$.

The buoyancy term is therefore calculated as follows:

$$\rho\beta(T-T_m)g_x=\frac{\rho\beta g_x}{C_p}(h-h_m)$$
$$h_{m,i}=\overline{h_{i,j}}=\left(\frac{1}{M-1}\sum_{j=2}^{M}h_{i,j}\right)_{i=2,L} \quad (19)$$

where j is the index in the radial direction and i in the axial one.

2.4. *The solution procedure*

The above equations, with appropriate initial and boundary conditions, are solved by a finite-difference procedure which we need describe here only in outline,

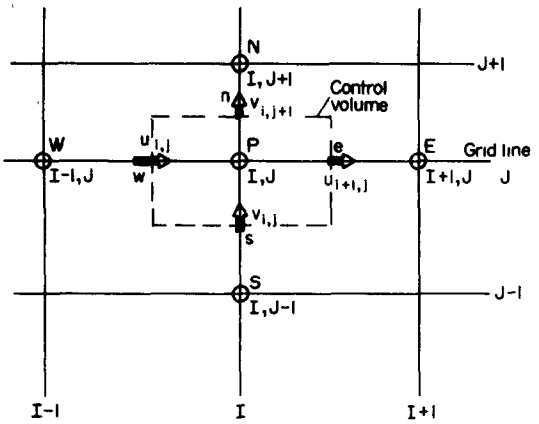

FIG. 2. Staggered grid system with indentification of indices.

a complete account of a similar procedure (but for parabolic flows) being given in Patankar and Spalding [1].

The grid layout used is a "staggered" grid system where the velocity components are stored midway between adjacent grid nodes whilst all the other variables are stored at the grid nodes themselves, as illustrated in Fig. 2.

The finite difference counterparts of the differential equations are obtained as follows. Integration of the partial differential equation governing the transport of each variable is performed, for each location of the variable, over the control volume that encloses this location. These integrations are performed after making presumptions about the manner in which the variable is distributed between grid nodes. For most purposes we assume that the variable under consideration varies in a stepwise manner between grid points; however, the convection and diffusion fluxes at a control-volume are calculated by assuming a linear variation of ϕ in the direction normal to that face.

Since an unsteady phenomenon is under study, we should consider the values of ϕ at the beginning of a time step (which are known), and those at the end of the step (which are to be calculated). A fully-implicit scheme is used, which means that the value of ϕ appearing in the convection and diffusion terms is taken to be the (unknown) value at the end of the time step.

The result of these operations is an algebraic equation for each grid location, representing the discretized form of the balance of the variable, over the control volume corresponding to that location. For a general dependent variable ϕ this equation takes the form (see also Fig. 2)

$$\sum_{i=E,W,N,S} A_i\phi_p - S_P\phi_P = \sum_{i=E,W,N,S} A_i\phi_i + A_P^0\phi_P^0 + S_U. \quad (20)$$

Where:
$$\begin{aligned} A_E &\equiv T_e^* - f_e L_e \\ A_W &\equiv T_W^* + (1-f_w)L_w \\ A_N &\equiv T_n^* - f_n L_n \\ A_S &\equiv T_s^* + (1-f_s)L_s \\ T_i &= \Gamma_i a_i/\delta_i \\ L_i &= \dot{m}_i'' a_i \end{aligned} \quad (21)$$

$$T_i^* \equiv \max[T_i, -(1-f_i)L_i, f_i L_i] \quad (21)$$

f_i are interpolation factors
a_i are control cell areas
δ_i are internodal distances
Γ_i are the diffusion coefficients.

S_P and S_U are the two parts of the linearised sources (and/or sinks) ($S = S_P\phi_P + S_U$), the superscript 0 denotes values at the beginning of the time step, Δt, and the subscript i takes on the values e, w, s, n (see Fig. 2).

Also:
$\dot{m}_i''$, is the mass flux crossing the cell face i, and

$$A_P^0 \equiv \max[M^0, (L_e - L_w + L_n - L_s)] \quad (22)$$

where

$$M \equiv 0.5\rho(r_s + r_n)\Delta x\Delta y/\Delta t \quad (23)$$

the r's being local radii of curvature.

A special treatment is applied to the momentum equations, developed by Spalding and co-workers [13–15] for parabolic flows, a key feature of

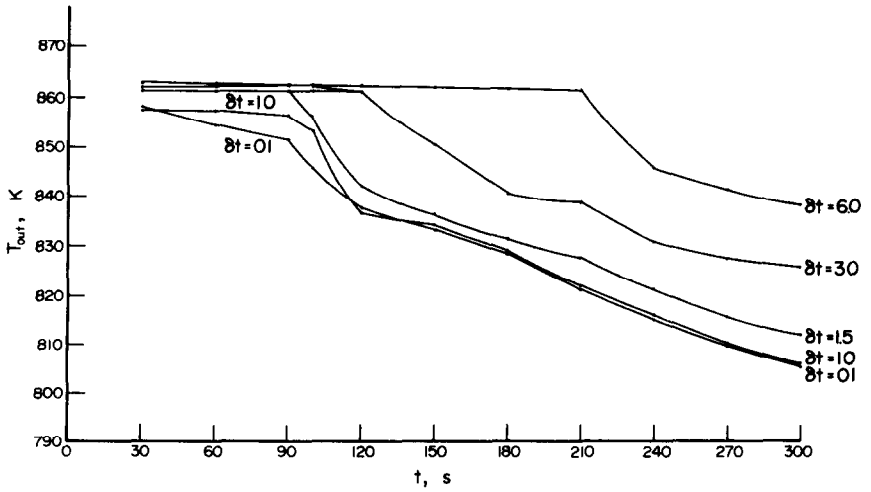

FIG. 3. Outlet temperature vs time. Optimisation of the time-step.

which is the so called SIMPLE (for Semi-Implicit-Method for Pressure-Linked Equations) algorithm. This yields a Poisson equation for the "pressure correction" which is used to update the velocity and pressure fields.

Hybrid differencing is used (Patankar and Spalding, [1]). The difference equations are solved in turn for each variable by the application of the tri-diagonal matrix algorithm.

An important aspect of the solution procedure concerns the treatment of the wall boundary conditions. The incorporation of the effects of the vicinity of a wall to turbulence proves expensive in computer time. One economical method of accounting for these effects is by way of "wall functions". These functions are based on some ideas of Spalding [13] and are embodied in algebraic expressions which force the numerical solution to behave in a specified manner. The wall functions for velocity components and for enthalpy are based on the assumption of a log-law in the vicinity of a wall. For k, a zero diffusive flux at the wall is used; this is consistent with the assumption of a fluid layer of uniform shear stress (which results in a log distribution of velocity). For ε the empirical evidence that a typical length scale of turbulence varies linearly with the distance from the wall, is used to calculate ε itself at the near wall point.

3. RESULTS AND DISCUSSIONS

3.1. *Computational details*

In the computations from which the following results were derived, the finite-difference grid possessed 16 intervals in the r direction and 16 intervals in the x direction. The grid spacing was non-uniform, the grid lines being more closely spaced near the walls than near the centre. That the 16×16 grid gave sufficient accuracy was confirmed by repeating the calculations with finer and coarser grids. As a matter of fact, it is only the variation of the turbulence variables (k, ε) near the boundaries that dictates such a fine grid.

A time step of 0.1 s for the first 100 s (reactor time) was used and then a time step of 1 s. That these time steps gave sufficient accuracy was confirmed by repeating the calculations with shorter and longer time steps; the results of some of these tests are shown in Fig. 3.

Using the above steps, the variability of the outlet temperatures is much less than 1%.

The computer time needed to establish the steady-state solution with the above grid was of the order of 100 s on a CDC 6600 computer. The transient calculations required on average about 2.5 s on a CDC 6600 computer, for every 1 s of reactor time.

3.2. *The flow and thermal fields*

The program is run for a number of iterations until steady-state is reached; then the time dependent terms are introduced and the program proceeds in time steps. The transient operation refers to the sodium stream entering the plenum at flow rates and inlet temperatures which are specified functions of time. The program was applied for three such prespecified functions. In all of them the flow rate is decreased to about 10% of full flow rate after about 250 s (reactor time) from the initiation of the transient. In the same time the inlet sodium temperature is decreased to about 75–80% of its value at the initiation of the transient. The difference of the three tested transients lies in the different shape of the inlet temperature vs time curves employed. Those transients were conveniently introduced into the program by finding analytic expressions for the given time curves by means of a polynomial fitting routine.

Figures 4–10 present the variation, for the three test cases, of some turbulence quantities, radially at the level of the outlet nozzles (A) and axially at the level of

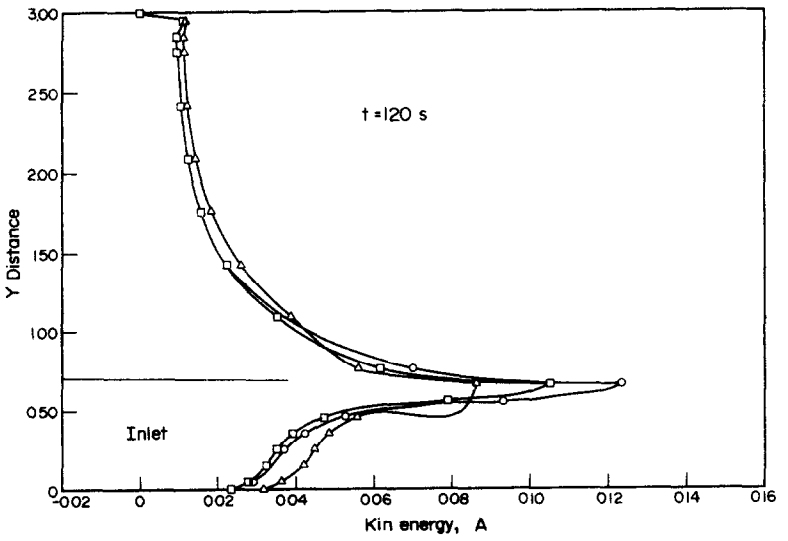

FIG. 4. Radial distribution of the turbulence kinetic energy at $t = 120$ s after the initiation of the transient.

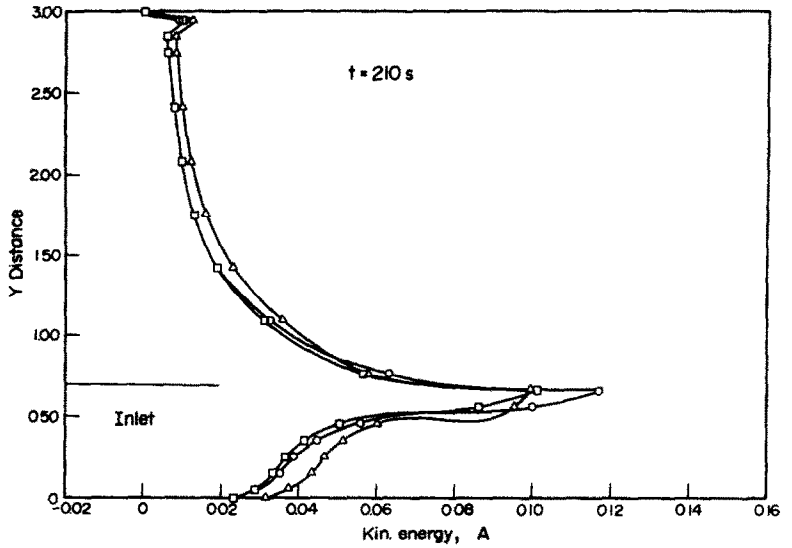

FIG. 5. Radial distribution of the turbulence kinetic energy at $t = 210$ s after the initiation of the transient.

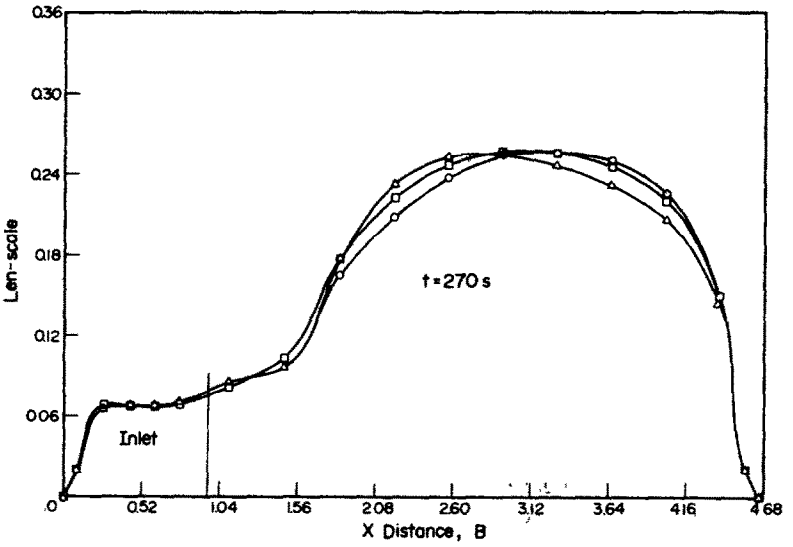

FIG. 6. Axial distribution of length scale at $t = 270$ s after the initiation of the transient.

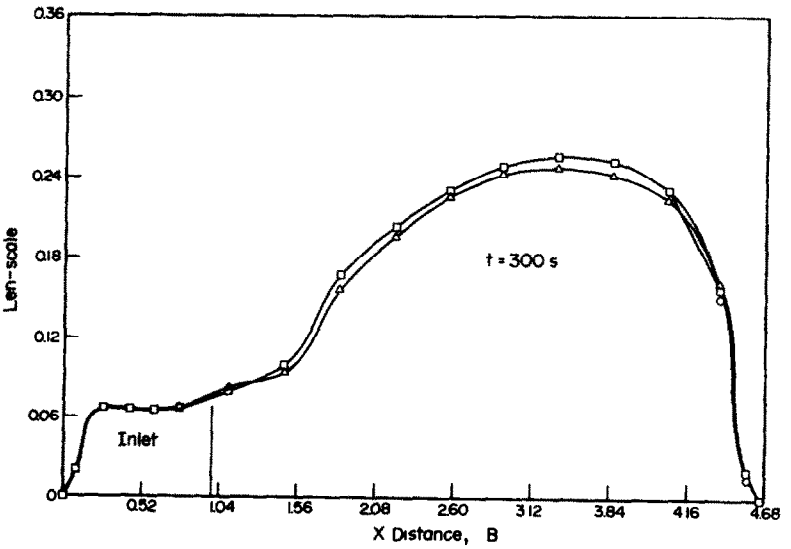

FIG. 7. Axial distribution of length scale at $t = 300$ s after the initiation of the transient.

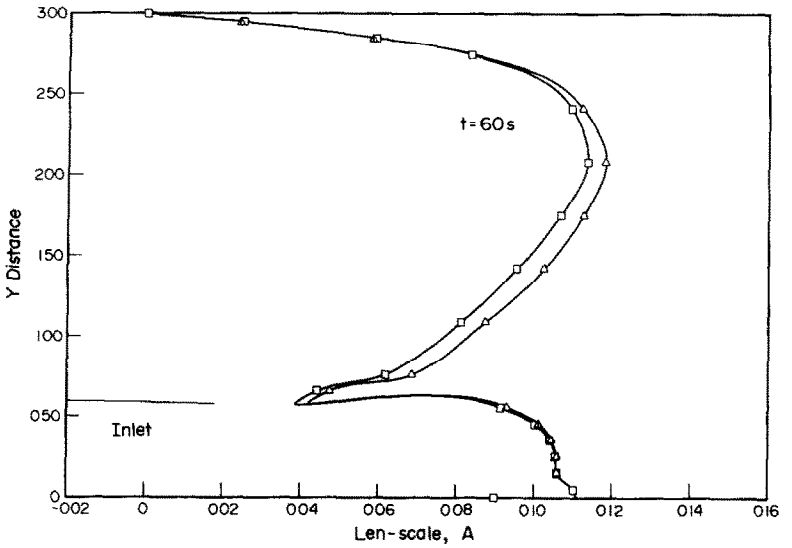

FIG. 8. Radial distribution of length scale at $t = 60$ s after the initiation of the transient.

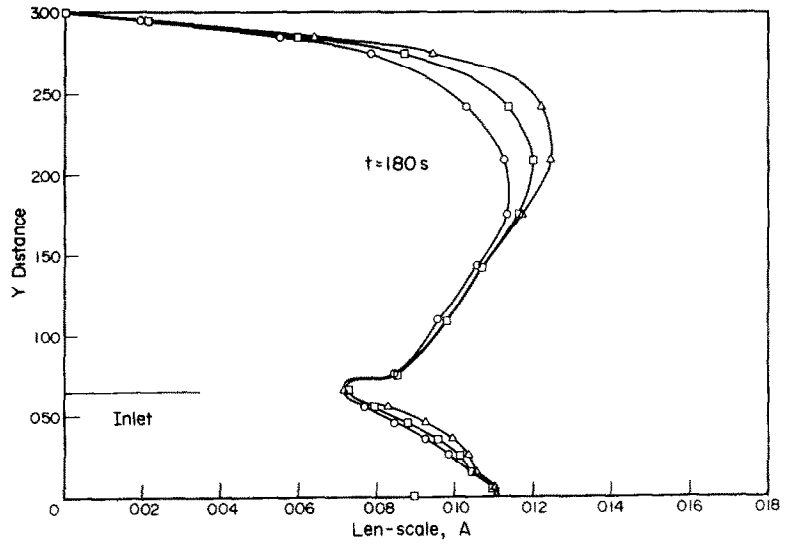

FIG. 9. Radial distribution of length scale at $t = 180$ s after the initiation of the transient.

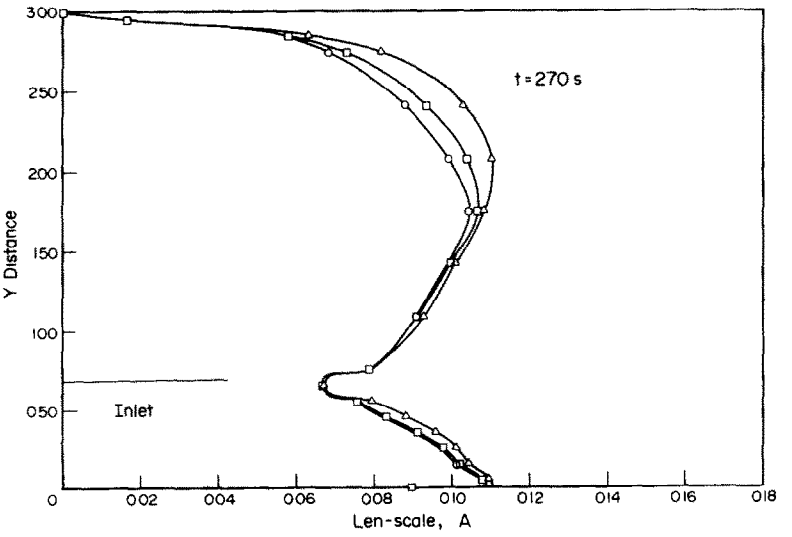

FIG. 10. Radial distribution of length scale at $t = 270$ s after the initiation of the transient.

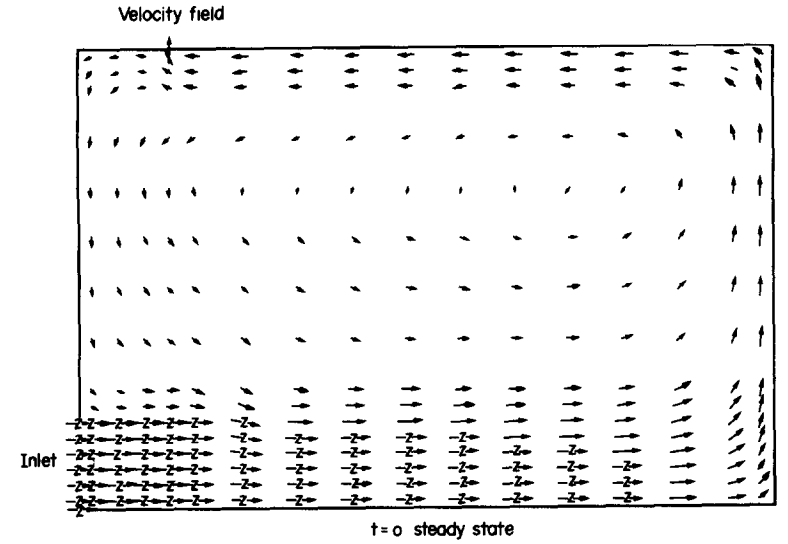

FIG. 11. Velocity vector field at $t = 0$ (steady-state).

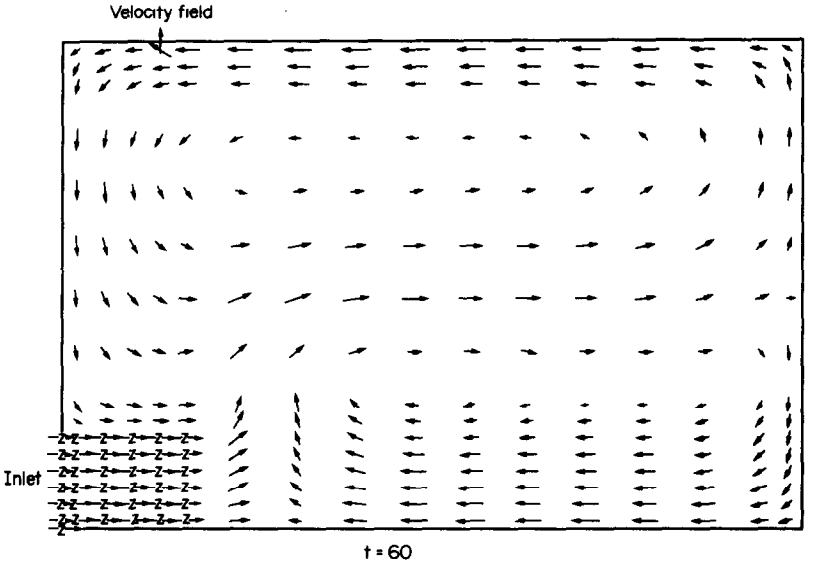

FIG. 12. Velocity vector field at $t = 60$ s after the initiation of the transient.

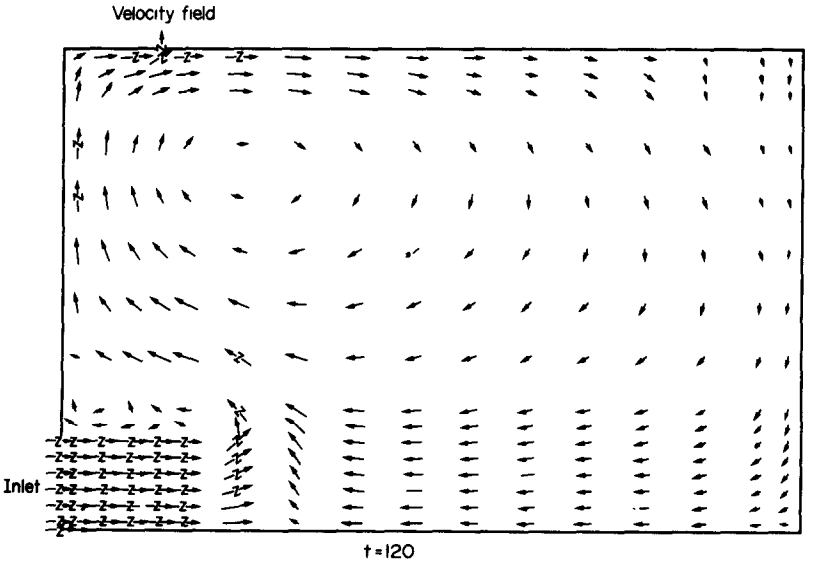

FIG. 13. Velocity vector field at $t = 120$ s after the initiation of the transient.

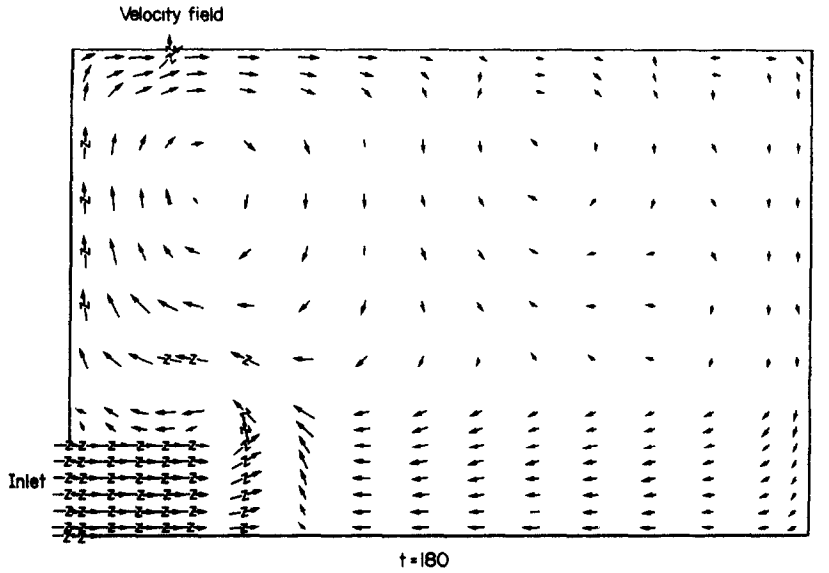

FIG. 14. Velocity vector field at $t = 180$ s after the initiation of the transient.

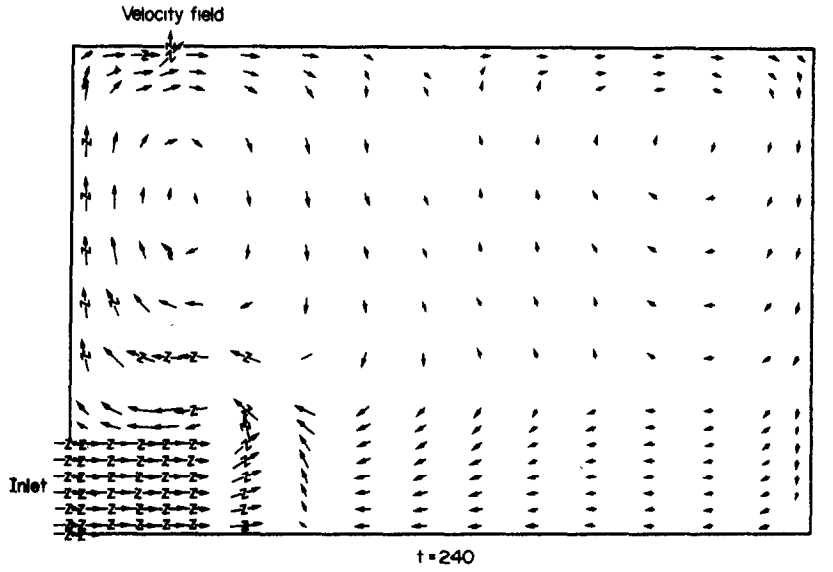

FIG. 15. Velocity vector field at $t = 240$ s after the initiation of the transient.

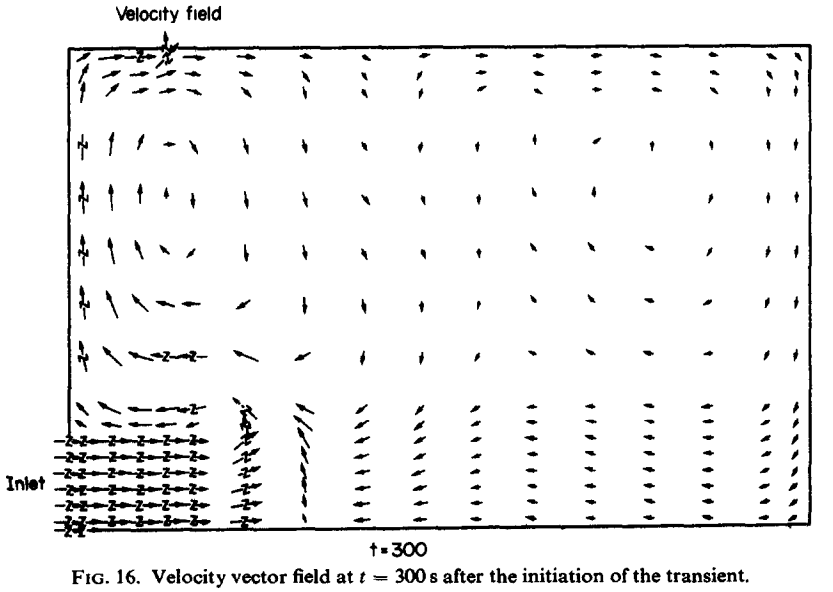

FIG. 16. Velocity vector field at $t = 300$ s after the initiation of the transient.

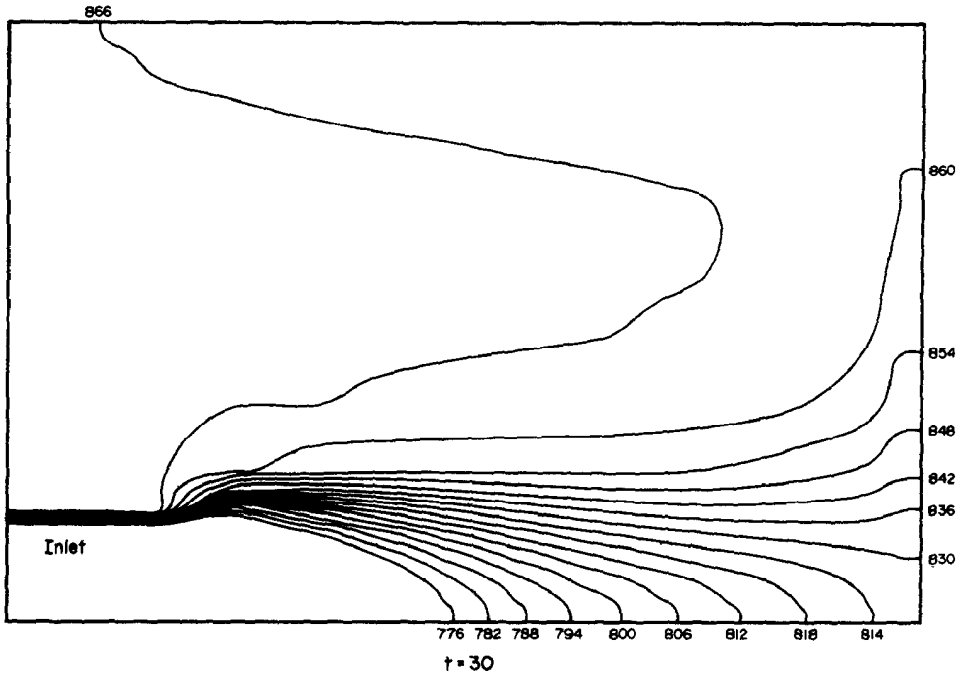

FIG. 17. Temperature contours (K) at $t = 30$ s after the initiation of the transient.

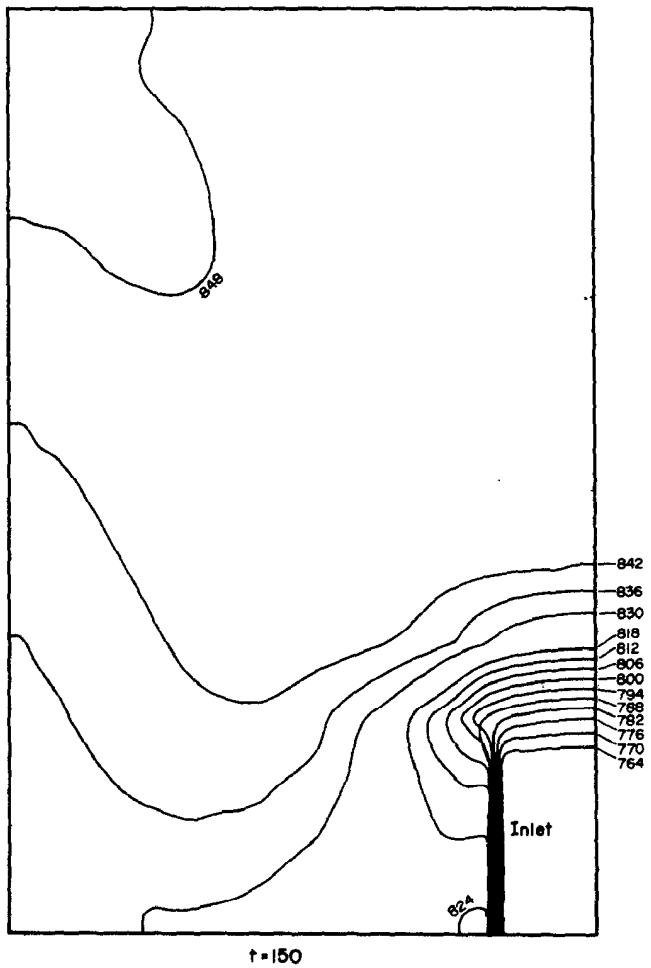

FIG. 18. Temperature contours (K) at $t = 150$ s after the initiation of the transient.

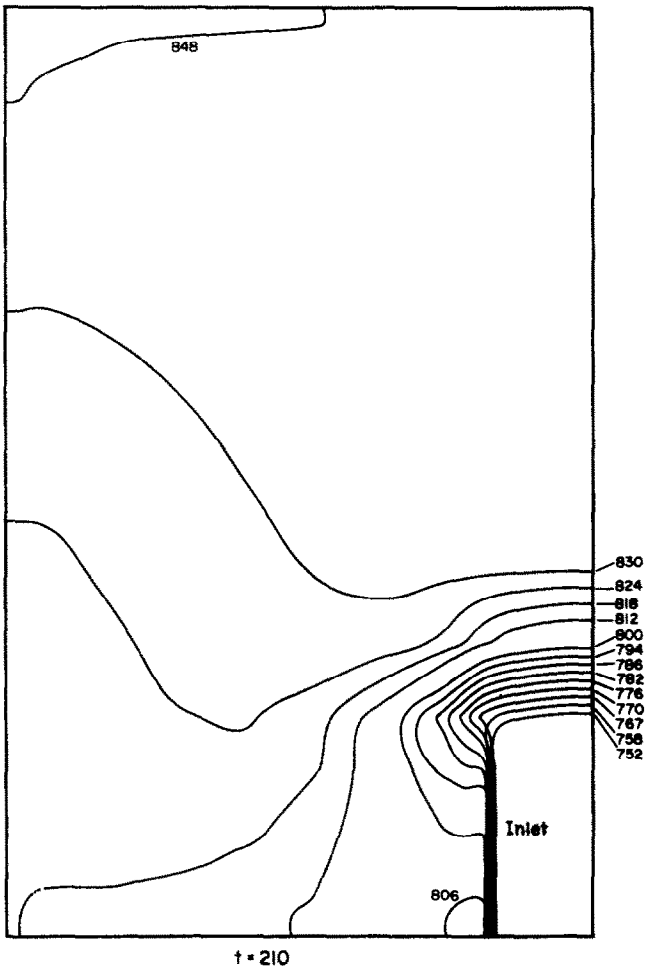

FIG. 19. Temperature contours (K) at $t = 210$ s after the initiation of the transient.

the first grid line next to the entrance tube (B) (see Fig. 1). The purpose of these figures is solely to show the plausible behaviour of the turbulence model employed. The presented turbulence variables are in good qualitative agreement with expectations.

Figure 11 shows the predicted steady-state velocity field. It is indicated that under steady-state isothermal conditions, the flow pattern within the plenum resembles a toroid.

In all runs, where the increase in density of the incoming fluid is accompanied by a flow coastdown to about 10% of the initial flow rate, flow stratification invariably occured. Upon entering the plenum the fluid was quickly forced downward and outward toward the exit nozzles. The predicted flow patterns are in good qualitative agreement with expectations and small-scale reactor experiments. Figures 12–16* present the predicted flow field for the transient every 60 s (reactor time) after its initiation.

Figures 17–20† present the temperature contours for a test run. Considering the apparent severity of the stratified flow pattern, an abrupt outlet nozzle thermal transient might be expected. However, Fig. 21 indicates a relatively modest outlet transient. Therefore a relatively large effective volume of the plenum is still active in mixing.

3.3. *Conclusions*

From the evidence of the computed results, it can be concluded that for all the test cases considered the flow pattern can be described as follows:

In the steady state, the coolant flows vertically upward, deflects horizontally at the top and then passes downward near the vessel wall toward the outlet. One large central eddy dominates the flow.

The flow can be characterised by a Rankine toroid driven at the inner opening with a jet emerging from the reactor. The fluid in the outlet plenum is initially circulating at normal operating conditions and when the reactor is "scrammed" the core jet velocities start to decrease and a new pattern develops.

Initially the core jet velocity becomes quite low, the

* We assign the maximum length not to the largest vector in the field, but to a vector equal to twice the average value of all the vectors present. If a vector is larger in magnitude than this maximum, we simply represent it by a line segment of the same size, on which we print a symbol z to distinguish it.

† The contours plotting routine is capable of producing only one curve per contour value.

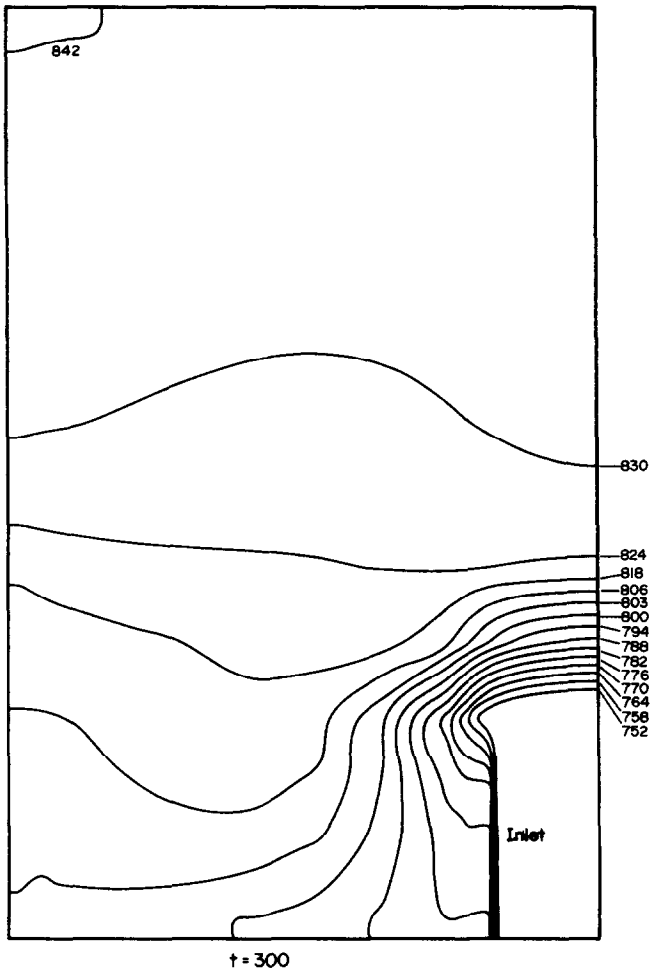

FIG. 20. Temperature contours (K) at $t = 300$ s after the initiation of the transient.

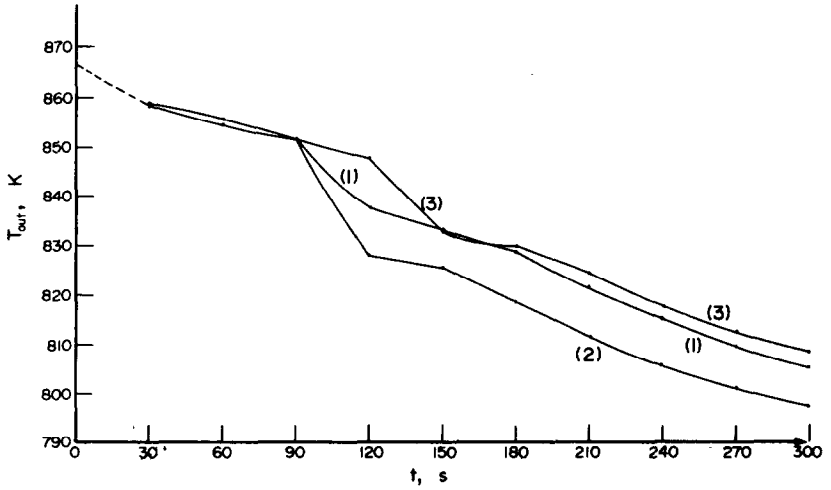

FIG. 21. Outlet temperature vs time for the three different transients used in the present study.

mixing zone collapses and the toroid slows up.

After some time the jet energy becomes less than the difference between the mixed mean temperature static differential head introduced by the temperature and the inlet temperature of the core outlet. The penetration of the jet decays and the toroid becomes stagnant. At this stage the lower velocity, denser fluid has insufficient inertia to overcome the negative buoyancy forces, and stratification occurs. Instead of penetrating well into the plenum and mixing with the fluid therein, the incoming jet is short-circuiting the plenum, being forced downward and outward, towards the outlet nozzles.

Despite the flow stratification, outlet nozzle tran-

effective volume of the plenum remains active in mixing. For the time period investigated (300 s) no new steady state pattern has yet been established.

4. CLOSURE

A finite-difference method has been successfully applied to the flow and heat transfer of liquid sodium coolant in the outlet plenum of a Fast Breeder Reactor. No numerical difficulties have been encountered and the computer times required are quite modest. The predictions appear satisfactory. Further tasks are the following: (i) extension of the method to the three-dimensional problem; (ii) incorporation of the components and instrument packages existing in the actual plenum; (iii) incorporation of the actual entrainment suppression plate at the top of the plenum.

REFERENCES

1. S. V. Patankar and D. B. Spalding, A calculation procedure for heat, mass transfer in three-dimensional parabolic flows, *Int. J. Heat Mass Transfer* **15**(10), 1787–1806 (1972).
2. F. H. Harlow and P. I. Nakayama, Transport of turbulence energy decay rate, Report LA-3854, Los Angeles Sci. Lab., University of California (1968).
3. B. E. Launder and D. B. Spalding, *Mathematical Models of Turbulence*. Academic Press, New York (1972).
4. D. B. Spalding, A two-equation model of turbulence, Commemorative Lecture for Prof. F. Boswajakovic, *ForschHft. Ver. Dt. Ing.* **546**, 5–16 (1972).
5. D. B. Spalding, Turbulence models and their experimental verification, Imperial College, M.E.D. HTS/73/19 (1973).
6. D. B. Spalding and D. G. Tatchell, A prediction procedure for flow, combustion and heat transfer close to the base of a rocket, Imperial College, London, Mechanical Engineering Dept., Heat Transfer Section, Report No. HTS/73/42 (1973).
7. A. D. Gosman, M. L. Koosinlin, F. C. Lockwood and D. B. Spalding, Transfer of heat in rotating systems, ASME, New Orleans, 76-GT-25 (1976).
8. E. K. H. Khalil, D. B. Spalding and J. H Whitelaw, The calculation of local flow properties in two-dimensional furnaces, *Int. J. Heat Mass Transfer* **18**, 775 (1975).
9. O. E. Dwyer, Eddy transport in liquid metal heat transfer, *A.I.Ch.E. Jl* **9**(2), 261–268 (1963).
10. J. R. Tyldesley and R. S. Silver, The prediction of the transport properties of a turbulent fluid, *Int. J. Heat Mass Transfer* **11**(9), 1325–1340 (1968).
11. V. M. Borishanski and T. B. Zablotskaya, High conductivity fluid flow turbulent heat transfer, *Atomn. Energ.* **22**(2), 135 (1967).
12. A. J. Reynolds, The prediction of turbulent Prandtl and Schmidt numbers, *Int. J. Heat Mass Transfer* **18**(9), 1055 (1975).
13. S. V. Patankar and D. B. Spalding, *Heat and Mass Transfer in Boundary Layers*, 2nd Edn. Intertext, London (1970).
14. D. B. Spalding, A novel-finite-difference formulation for differential expressions involving both first and second derivatives, *Int. J. Numer. Meth. Engng* **4**, 551–559 (1972).
15. D. B. Spalding, The calculation of convective heat transfer in complex flow systems, in *Proceedings of the Fifth International Heat Transfer Conference*, Vol. 5, pp. 44–60. Science Council of Japan, Tokyo (1974).

ECOULEMENT ET TRANSFERT THERMIQUE TRANSITOIRE DE SODIUM LIQUIDE REFRIGERANT DANS LE VOLUME SUPERIEUR DE LA CUVE D'UN REACTEUR A NEUTRONS RAPIDES

Résumé—On applique une procédure de calcul des écoulements elliptiques et axisymétriques pour estimer les champs transitoires de vitesse et de température dans un jet de fluide lourd pénétrant verticalement dans un volume de fluide relativement léger. Cette situation est rencontrée dans le volume supérieur de la cuve d'un surgénérateur refroidi par métal liquide (L M F B R) pendant le régime transitoire. Les équations de bilan de quantité de mouvement et de chaleur sont résolues sur un ordinateur CDC 6600 pour différentes conditions dans le volume inférieur de la cuve, à partir d'un modèle de turbulence à deux équations et d'une modélisation convenable des termes de gravité. Des prévisions d'écoulement et de transfert thermique sont présentés graphiquement sous forme de cartes des vecteurs vitesse et de contours de température. Les prévisions sont en accord qualitatif avec les estimations lesquelles considèrent que l'écoulement by-passe invariablement le volume supérieur de la cuve.

INSTATIONÄRE STRÖMUNG UND WÄRMEÜBERGANG VON FLÜSSIGEM NATRIUM ALS KÜHLMITTEL IM AUSLASSPLENUM EINES SCHNELLEN BRUTREAKTORS

Zusammenfassung—Zur Beschreibung des instationären Geschwindigkeits- und Temperaturfeldes eines schweren Fluidstroms, der senkrecht in das Volumen eines relative leichten Fluids gespritzt wird, wurde ein Berechnungsverfahren für achsensymmetrische elliptische Strömung angewendet. Dieser Zustand tritt im Auslaßplenum eines flüssigkeitsgekühlten Schnellen Brüters (LMFBR) während instationärer Betriebszustände des Reaktors auf. Die über der Zeit gemittelten Erhaltungsgleich ungen für Impuls und Wärmeübergang wurden auf einer CDC 6600-Rechenanlage für verschiedene Eintrittstransienten des Plenums mit Hilfe eines Turbulenzmodells (beschrieben durch zwei Gleichungen) bei geeigneten Annahmen für die Auftriebs-Terme berechnet. Es werden Voraussagen über die Strömung und den Wärmeübergang in Form von Bildern des Geschwindigkeitsvektors und der Temperaturverteilung gemacht. Die Berechnungen stimmen qualitativ gut mit den Erwartungen überein und zeigen einheitlich, daß die Strömung das Auslaßplenum passiert.

НЕСТАЦИОНАРНОЕ ТЕЧЕНИЕ И ТЕПЛООБМЕН ЖИДКОГО НАТРИЕВОГО ТЕПЛОНОСИТЕЛЯ В КАМЕРЕ НА ВЫХОДЕ ИЗ БЫСТРОГО ЯДЕРНОГО РЕАКТОРА

Аннотация — Методика расчёта эллиптических уравнений, описывающих осесимметричные потоки, используется для расчёта нестационарных полей скорости и температуры струи тяжёлой жидкости, втекающей вертикально в объём с более лёгкой жидкостью. Такая ситуация наблюдается в камере на выходе из быстрого реактора-размножителя с жидкометаллическим теплоносителем в переходных режимах. Усредненные во времени уравнения сохранения импульса и переноса тепла решались на цифровой вычислительной машине CDC 6600 для различных переменных параметров на входе в камере с использованием модели турбулентности, описываемой двумя уравнениями, и соответствующей аппроксимации свободноконвективного члена. Расчётные данные по течению и теплообмену представлены в виде графиков для вектора скорости и распределений температуры. Результаты расчётов качественно согласуются с ожидавшимися данными и свидетельствуют о том, что происходит проскок потока в камере на выходе из реактора.